Inorg. Chem. **2008**, *47*, 373–380

First-Row Transition Metal–Halide Complexes Supported by a Monoanionic [N_2P_2] Ligand

Wayne A. Chomitz, Seth F. Mickenberg, and John Arnold*

Department of Chemistry, University of California, Berkeley, California 94720-1460

Received August 24, 2007

Metal–halide complexes of a multidentate monoanionic ligand ^{t}BuN(H)SiMe$_2$N(CH$_2$CH$_2$P^{i}Pr$_2$)$_2$, H[N_2P_2], with Ti, V, Cr, Mn, Fe, Co, and Ni have been isolated and characterized. X-ray crystallographic studies were performed on [N_2P_2]TiCl$_2$ (**3**), [N_2P_2]CrCl$_2$ (**5**), [N_2P_2]MnCl (**6**), [N_2P_2]FeCl (**7**), [N_2P_2]CoCl (**8**), and [N_2P_2]NiBr (**9**), and the results revealed that the [N_2P_2] ligand exhibits considerable flexibility in the manner in which it binds to first-row metals and that three distinct coordination modes are observed: κ^3-N_2P (Ti), κ^3-NP_2 (Mn, Fe, Co), and κ^4-N_2P_2 (Cr, Ni). Electrochemical (CV) data and room-temperature magnetic susceptibilities are also described.

Introduction

Ligand design has played an important role in the development of new reactivity patterns at metal centers. Typically, ligands are chosen on a metal-by-metal basis, and their steric and electronic properties are tailored to the particular metal in question. By tuning the denticity of these ligands, the appropriate number of donors with suitable electronic properties (e.g., hardness or softness) for a particular metal can be achieved, as well as steric control at the metal center. These fundamental concepts have led to the discovery of a wide range of interesting compounds, many of which demonstrate unusual reactivity patterns. The introduction of the ligand $^-$N(SiMe$_2$CH$_2$PR$_2$)$_2$, (^{R}PNP), by Fryzuk and co-workers demonstrated how a ligand set containing both hard and soft donors could stabilize early, middle, and late transition-metal complexes.[1−8] The implementation of this general ligand type has led to the isolation of new and interesting compounds including the first zirconium side-on bound dinitrogen compound, [(^{R}PNP)-ZrCl]$_2$(μ-η^2:η^2-N$_2$),[9] the only structurally characterized zirconium alkylidene complex, [P_2Cp]Zr=CHPh(Cl)[10] where [P_2Cp] = [η^5-C$_5$H$_3$-1,3-(SiMe$_2$CH$_2$P^{i}Pr$_2$)$_2$], and the 16 e$^-$ iridium methylidene compound (^{R}PNP)Ir=CH$_2$[11] (Figure 1a). Since its introduction, other research groups have examined the coordination and substitution chemistry of complexes supported by (^{R}PNP) ligands and related ligand sets leading to a number of fascinating results. Caulton and co-workers have isolated and characterized a four-coordinate Ru(II)[12] and a terminal Ru(IV) nitride[13] as well as a three-coordinate Co(I) complex[14,15] in addition to a number of interesting rhenium[16] and osmium[17] compounds supported by (^{R}PNP), where R = ^{t}Bu. The alternative ligand set [PNP], where [PNP] = $^-$N(CH$_2$CH$_2$PR$_2$)$_2$, has been used by Edwards and co-workers to support a range of early metal and actinide

* To whom correspondence should be addressed. E-mail: arnold@berkeley.edu.

(1) Fryzuk, M. D.; Haddad, T. S. *J. Am. Chem. Soc.* **1988**, *110*, 8263−8265.
(2) Fryzuk, M. D.; Macneil, P. A.; Rettig, S. J. *Organometallics* **1986**, *5*, 2469−2476.
(3) Fryzuk, M. D.; Carter, A.; Westerhaus, A. *Inorg. Chem.* **1985**, *24*, 642−648.
(4) Fryzuk, M. D.; Macneil, P. A. *J. Am. Chem. Soc.* **1981**, *103*, 3592−3593.
(5) Fryzuk, M. D.; Leznoff, D. B.; Ma, E. S. F.; Rettig, S. J.; Young, V. G. *Organometallics* **1998**, *17*, 2313−2323.
(6) Fryzuk, M. D.; Leznoff, D. B.; Thompson, R. C.; Rettig, S. J. *J. Am. Chem. Soc.* **1998**, *120*, 10126−10135.
(7) Fryzuk, M. D.; Giesbrecht, G.; Rettig, S. J. *Organometallics* **1996**, *15*, 3329−3336.
(8) Fryzuk, M. D.; Giesbrecht, G. R.; Olovsson, G.; Rettig, S. J. *Organometallics* **1996**, *15*, 4832−4841.
(9) Fryzuk, M. D.; Haddad, T. S.; Rettig, S. J. *J. Am. Chem. Soc.* **1990**, *112*, 8185−8186.
(10) Fryzuk, M. D.; Mao, S. S. H.; Zaworotko, M. J.; Macgillivray, L. R. *J. Am. Chem. Soc.* **1993**, *115*, 5336−5337.
(11) Fryzuk, M. D.; Gao, X. L.; Joshi, K.; Macneil, P. A.; Massey, R. L. *J. Am. Chem. Soc.* **1993**, *115*, 10581−10590.
(12) Watson, L. A.; Ozerov, O. V.; Pink, M.; Caulton, K. G. *J. Am. Chem. Soc.* **2003**, *125*, 8426−8427.
(13) Walstrom, A.; Pink, M.; Yang, X. F.; Tomaszewski, J.; Baik, M. H.; Caulton, K. G. *J. Am. Chem. Soc.* **2005**, *127*, 5330−5331.
(14) Ingleson, M.; Fan, H. J.; Pink, M.; Tomaszewski, J.; Caulton, K. G. *J. Am. Chem. Soc.* **2006**, *128*, 1804−1805.
(15) Ingleson, M. J.; Pink, M.; Caulton, K. G. *J. Am. Chem. Soc.* **2006**, *128*, 4248−4249.
(16) Ozerov, O. V.; Huffman, J. C.; Watson, L. A.; Caulton, K. G. *Organometallics* **2003**, *22*, 2539−2541.
(17) Lee, J. H.; Pink, M.; Caulton, K. G. *Organometallics* **2006**, *25*, 802−804.

10.1021/ic701670u CCC: $40.75
Published on Web 12/01/2007

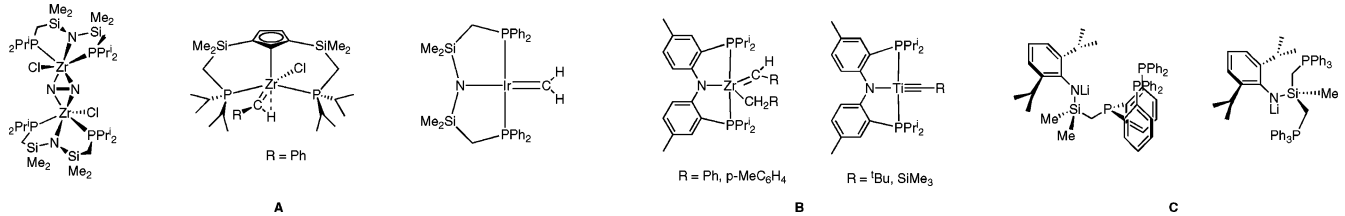

Figure 1. Examples of monoanionic ligands incorporating neutral phosphines.

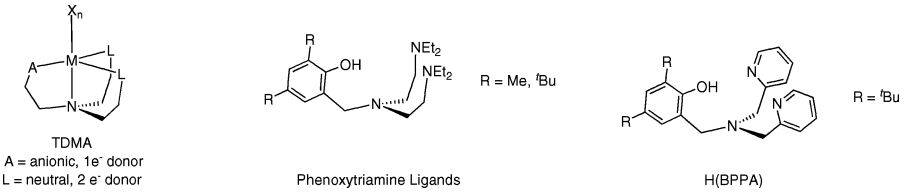

Figure 2. General TDMA ligand motif and previously examined examples.

coordination compounds.[18−24] More recently, [PNP]-supported chromium complexes have proven effective as ethylene trimerization catalysts.[25] Further modification by incorporating a phenylene backbone has led to a more rigid PNP ligand, and this ligand has proven effective at supporting a zirconium alkylidene[26] as well as a titanium alkylidene and alkylidyne[27] (Figure 1b). Alternative "mixed" hard−soft ligands, [$^{Si}NP_2$] and [$^{Si}NP_3$], have been adopted by Peters and co-workers, and they have shown that these ligands bind iron and cobalt in different coordination modes depending on the electronic requirements of the metal center[28] (Figure 1c).

We previously reported the use of tetradentate monoanionic (TDMA) ligands for use with yttrium in lactide polymerization.[29] Our effort to expand TDMA chemistry using phenoxytriamine ligands to other metals by salt metathesis reactions was hampered by the observation of low yields and intractable mixtures. The modular nature of the TDMA framework allows for simple design modifications to test the resulting steric and electronic consequences on complex structure and reactivity. To this end, the effect of replacing the two diethylamine donors with pyridines was examined[30] (Figure 2). Though a number of main group and early metal−halide complexes were easily synthesized, metal alkyl derivatives were subject to decomposition by deprotonation of a 2-picolyl proton, resulting in the transformation of BPPA from a monoanionic to a dianionic ligand.[30,31] In an effort to capitalize on the previous success of ligands incorporating hard and soft moieties, we believed introducing neutral phosphine donors into the TDMA ligand motif would enhance the stability of the resulting metal alkyl complexes and open up new avenues to synthesizing low-valent metal species. In addition, we substituted the phenoxy anionic group with an amide donor for ease of synthesis. The resulting ligand exhibits the unusual ability to change its coordination mode to accommodate the electronic requirements of the metal center with three distinct coordination modes (κ^3-N_2P, κ^3-NP_2, and κ^4−N_2P_2) being observed. Here, we report on the synthesis, coordination chemistry, and electrochemical properties of seven new first-row transition-metal complexes supported by ^{t}BuN(H)SiMe$_2$N(CH$_2$CH$_2$P^{i}Pr$_2$)$_2$, H[N_2P_2].

Experimental Section

All reactions were performed using standard Schlenk-line techniques or in an MBraun drybox (<1 ppm O_2/H_2O) unless noted otherwise. All glassware, cannulae, and Celite were stored in an oven at >425 K. Pentane, toluene, methylene chloride, diethyl ether, tetrahydrofuran (THF), and 1,2-dimethoxyethane (DME) were purified by passage through a column of activated alumina and degassed with nitrogen prior to use.[32] Deuterated solvents were vacuum transferred from sodium/benzophenone (benzene) or calcium hydride (chloroform). NMR spectra were recorded at ambient temperature on Bruker AV-300, AVQ-400, AVB-400, and DRX-500 spectrometers. ^{1}H and ^{13}C{^{1}H} chemical shifts are given relative to residual solvent peaks, and coupling constants (*J*) are given in hertz. ^{31}P{^{1}H} chemical shifts are referenced to an external standard of P(OMe)$_3$ set to 1.67 ppm. Infrared samples were prepared as Nujol mulls and taken between KBr disks. Magnetic susceptibility (μ_{eff}) values were determined using solid samples in a Johnson Matthey magnetic susceptibility balance. Melting points

(18) Coles, S. J.; Danopoulos, A. A.; Edwards, P. G.; Hursthouse, M. B.; Read, P. W. *J. Chem. Soc., Dalton Trans.* **1995**, 3401−3408.
(19) Coles, S. J.; Edwards, P. G.; Hursthouse, M. B.; Read, P. W. *J. Chem. Soc., Chem. Commun.* **1994**, 1967−1968.
(20) Alsoudani, A. R. H.; Batsanov, A. S.; Edwards, P. G.; Howard, J. A. K. *J. Chem. Soc., Dalton Trans.* **1994**, 987−995.
(21) Alsoudani, A. R. H.; Edwards, P. G.; Hursthouse, M. B.; Malik, K. M. A. *J. Chem. Soc., Dalton Trans.* **1995**, 355−361.
(22) Danopoulos, A. A.; Edwards, P. G. *Polyhedron* **1989**, *8*, 1339−1344.
(23) Danopoulos, A. A.; Edwards, P. G.; Parry, J. S.; Wills, A. R. *Polyhedron* **1989**, *8*, 1767−1769.
(24) Danopoulos, A. A.; Wills, A. R.; Edwards, P. G. *Polyhedron* **1990**, *9*, 2413−2418.
(25) McGuinness, D. S.; Wasserscheid, P.; Keim, W.; Hu, C. H.; Englert, U.; Dixon, J. T.; Grove, C. *Chem. Commun.* **2003**, 334−335.
(26) Weng, W.; Yang, L.; Foxman, B. M.; Ozerov, O. V. *Organometallics* **2004**, *23*, 4700−4705.
(27) Bailey, B. C.; Fan, H. J.; Baum, E. W.; Huffman, J. C.; Baik, M. H.; Mindiola, D. J. *J. Am. Chem. Soc.* **2005**, *127*, 16016−16017.
(28) Whited, M. T.; Rivard, E.; Peters, J. C. *Chem. Commun.* **2006**, 1613−1615.
(29) Westmoreland, I.; Arnold, J. *Dalton Trans.* **2006**, 4155−4163.
(30) Chomitz, W. A.; Minasian, S. G.; Sutton, A. D.; Arnold, J. *Inorg. Chem.* **2007**, *47*, 7199−7209.
(31) Marinescu, S. C.; Agapie, T.; Day, M. W.; Bercaw, J. E. *Organometallics* **2007**, *26*, 1178−1190.
(32) Alaimo, P. J.; Peters, D. W.; Arnold, J.; Bergman, R. G. *J. Chem. Educ.* **2001**, *78*, 64−64.

were determined using sealed capillaries prepared under nitrogen and are uncorrected. $TiCl_3(THF)_3$,[33] $VBr_3(THF)_3$,[34] $CrCl_3(THF)_3$,[35] $[(TMEDA)FeCl_2]_2$,[36] and Li[PNP][22] were prepared using the literature procedures, and unless otherwise noted all reagents were acquired from commercial sources. Elemental analyses and mass spectral data were determined at the College of Chemistry, University of California, Berkeley. The X-ray structural determination was performed at CHEXRAY, University of California, Berkeley. Electrochemical measurements were performed using a BAS-100b electrochemical analyzer with a BAS C3 cell stand mounted on the bench top. Experiments were performed in dichloromethane with [nBu$_4$N][PF_6] (0.3 M) as the supporting electrolyte at ambient temperature (22 °C) under N_2. A three-electrode setup was implemented with a glassy-carbon working electrode, platinum auxiliary electrode, and a Ag/AgCl reference electrode. All potentials are reported relative to the Fc/Fc^+ couple as an internal standard.

H[N_2P_2] (1). To a solution of $ClSiMe_2NH^tBu$ (3.4 g, 21 mmol) in 70 mL of pentane was added a solution of Li[PNP] (6.1 g, 20 mmol) in 50 mL of pentane dropwise at room temperature. The solution was stirred for 12 h, filtered, and the remaining solid washed with pentane (30 mL). Volatiles were removed in vacuo leaving spectroscopically pure product as a colorless oil (7.8 g, 91% yield). H[N_2P_2] thus prepared was used without further purification. ^{1}H NMR (400 MHz, $CDCl_3$): δ 0.028 (s, 6 H, Si(CH_3)$_2$), 1.05 (m, 24 H, PCH(CH_3)$_2$), 1.15 (s, 9 H, ^{t}Bu), 1.43 (m, 4 H, PCH(CH$_3$)$_2$), 1.68 (m, 4 H, NCH$_2$CH_2P), 2.89 (m, 4 H, NCH_2-CH$_2$P). ^{13}C{^{1}H} NMR (125 MHz, $CDCl_3$): δ 0.92 (s), 18.67 (m), 20.08 (d), 22.34 (m), 23.01 (d), 33.53 (d), 45.09 (m), 48.91 (d). ^{31}P{^{1}H} NMR (400 MHz, $CDCl_3$): δ −1.0 (s). IR (cm^{-1}): 1363 (s); 1297 (w); 1250 (s); 1227 (s); 1198 (w); 1108 (m); 1054 (m); 1019 (m); 920 (m); 879 (w); 833 (s); 774 (s); 681 (m); 487 (w); 412 (m).

Li[N_2P_2] (2). To a solution of **1** (11 g, 25 mmol) in 50 mL of pentane was added 2.9 M BuLi (9.3 mL, 27 mmol) at −40 °C. The solution was allowed to warm to room temperature and stirred for 4 h. The solution was concentrated under vacuum until precipitation of crystalline material was observed. Cooling to −40 °C resulted in the isolation of colorless crystals (9.2 g, 83% yield). ^{1}H NMR (500 MHz, C_6D_6): δ 0.50 (s, 6 H, Si(CH_3)$_2$), 1.09 (m, 24 H, PCH(CH_3)$_2$), 1.55 (s, 9 H, ^{t}Bu), 1.64 (m, 8 H, PCH(CH$_3$)$_2$ and NCH$_2$CH_2P), 3.25 (m, 4 H, NCH_2CH$_2$P). ^{13}C{^{1}H} NMR (125 MHz, C_6D_6): δ 6.39 (s), 19.53 (d), 19.94 (d), 20.63 (d), 24.00 (d), 38.31 (s), 44.23 (d), 52.22 (s). ^{31}P{^{1}H} NMR (500 MHz, C_6D_6): δ −3.40 (s). IR (cm^{-1}): 1412 (w); 1354 (m); 1297 (m); 1247 (s); 1220 (m); 1192 (s); 1152 (w); 1096 (m); 1076 (m); 1056 (s); 1020 (m); 994 (w); 967 (w); 909 (m); 879 (w); 842 (s); 825 (s); 794 (m); 761 9s); 700 (m); 649 (m); 605 (w); 514 (w); 496 (m). Anal. Calcd for $H_{51}C_{22}N_2P_2SiLi$: C, 59.95; H, 11.69; N, 6.36. Found: C, 60.14; H, 11.67; N, 6.67. Mp = 115−116 °C.

[N_2P_2]TiCl$_2$ (3). To a blue suspension of $TiCl_3(THF)_3$ (0.25 g, 0.68 mmol) in 10 mL of toluene was added a solution of **2** (0.30 g, 0.68 mmol) in 5 mL of toluene dropwise at room temperature. The solution was stirred for 4 h over which time the solution became orange. The reaction mixture was filtered and concentrated until precipitation of crystalline material was observed. Storage at −40 °C resulted in the formation of turquoise crystals (0.21 g, 56% yield). IR (cm^{-1}): 1359 (s); 1296 (m); 1251 (s); 1225 (m); 1200 (s); 1104 (m); 1040 (s); 1016 (s); 944 (w); 924 (w); 891 (s); 850 (s); 822 (m); 802 (m); 775 (s); 750 (s); 666 (m); 640 (m); 615 (m); 546 (m); 525 (m); 502 (m); 463 (m); 424 (m). Anal. Calcd for $H_{51}C_{22}N_2P_2SiTiCl_2$: C, 47.82; H, 9.32; N, 5.07. Found: C, 47.68; H, 9.33; N, 5.42. Mp = 146−147 °C. μ_{eff} = 1.3 μ_B.

[N_2P_2]VBr$_2$ (4). To a red-brown suspension of $VBr_3(THF)_3$ (0.35 g, 0.68 mmol) in 10 mL of toluene was added a solution of **2** (0.30 g, 0.68 mmol) in 5 mL of toluene dropwise at room temperature. The solution was stirred for 5 h over which time the solution became purple-red. The solvent was removed in vacuo, and the product was extracted with methylene chloride. Following filtration through a bed of Celite and the removal of solvent under vacuum, **4** was dissolved in THF, and the resulting solution was concentrated and cooled to −40 °C, resulting in the formation of blue needles (0.24 g, 54% yield). IR (cm^{-1}): 1406 (w); 1360 (m); 1292 (w); 1252 (s); 1224 (m); 1196 (m); 1052 (m); 1032 (w); 1015 (s); 943 (w); 884 (m); 848 (s); 823 (w); 812 (w); 798 (w); 778 (m); 764 (m); 667 (m); 641 (w); 613 (w); 530 (m); 498 (w). Anal. Calcd for $H_{51}C_{22}N_2P_2SiVBr_2$: C, 40.99; H, 7.99; N, 4.35. Found: C, 41.01; H, 8.09; N, 4.68. Mp = 183−185 °C. μ_{eff} = 2.7 μ_B.

[N_2P_2]CrCl$_2$ (5). To a purple suspension of $CrCl_3(THF)_3$ (0.26 g, 0.68 mmol) in 10 mL of toluene was added a solution of **2** (0.30 g, 0.68 mmol) in 5 mL of toluene dropwise at room temperature. The solution was stirred for 12 h over which time the solution became dark green. The solvent was removed in vacuo, and the product was extracted with diethyl ether. The resulting solution was concentrated and cooled to −40 °C, resulting in the formation of dark purple blocks (0.18 g, 48% yield). IR (cm^{-1}): 1364 (s); 1350 (s); 1246 (m); 1225 (m); 1189 (s); 1062 (m); 1039 (m); 1016 (w); 995 (s); 970 (m); 924 (w); 912 (w); 883 (w); 851 (s); 802 (m); 781 (m); 764 (s); 741 (s); 693 (w); 656 (m); 567 (m); 506 (w); 476 (m); 442 (m). Anal. Calcd for $H_{51}C_{22}N_2P_2SiCrCl_2$: C, 47.46; H, 9.25; N, 5.03. Found: C, 47.44; H, 8.88; N, 5.40. Mp = 183−184 °C. μ_{eff} = 3.9 μ_B.

[N_2P_2]MnCl (6). To a suspension of $MnCl_2$ (0.086 g, 0.68 mmol) in 10 mL of DME was added a solution of **2** (0.30 g, 0.68 mmol) in 5 mL of DME dropwise at room temperature. The solution was stirred for 12 h. Following the removal of solvent under vacuum, the product was extracted with toluene, and the resulting solution was concentrated and cooled to −40 °C, resulting in the formation of colorless crystalline material (0.20 g, 56% yield). IR (cm^{-1}): 1348 (m); 1242 (m); 1224 (m); 1202 (m); 1056 (s); 1036 (m); 938 (w); 903 (m); 846 (s); 818 (m); 793 (w); 761 (m); 735 (m); 657 (w); 608 (w); 528 (w); 499 (w); 476 (w). Anal. Calcd for $H_{51}C_{22}N_2P_2SiMnCl$: C, 50.41; H, 9.83; N, 5.35. Found: C, 50.02; H, 10.06; N, 5.06. Mp = 153−154 °C. μ_{eff} = 5.8 μ_B.

[N_2P_2]FeCl (7). To a yellow suspension of $[FeCl_2(TMEDA)]_2$ (0.17 g, 0.34 mmol) in 10 mL of toluene was added a solution of **2** (0.30 g, 0.68 mmol) in 5 mL of toluene dropwise at room temperature. The solution was stirred for 12 h over which time the solution became orange. The reaction mixture was filtered and cooled to −40 °C, resulting in the formation of yellow needles (0.22 g, 61% yield). IR (cm^{-1}): 1349 (m); 1309 (w); 1240 (s); 1200 (s); 1095 (s); 1050 (s); 1017 (m); 917 (w); 929 (w); 884 (w); 848 (s); 798 (m); 757 (m); 739 (m); 685 (w); 657 (w); 603 (w); 528 (w). Anal. Calcd for $H_{51}C_{22}N_2P_2SiFeCl$: C, 50.32; H, 9.81; N, 5.34. Found: C, 50.03; H, 9.90; N, 5.63. Mp = 221−223 °C. μ_{eff} = 4.9 μ_B.

[N_2P_2]CoCl (8). To a blue suspension of $CoCl_2$ (0.088 g, 0.68 mmol) in 10 mL of DME was added a solution of **2** (0.30 g, 0.68 mmol) in 5 mL of DME dropwise at room temperature. The solution

(33) Jones, N. A.; Liddle, S. T.; Wilson, C.; Arnold, P. L. *Organometallics* **2007**, *26*, 755−757.
(34) Davies, S. C.; Durrant, M. C.; Hughes, D. L.; Le Floc'h, C.; Pope, S. J. A.; Reid, G.; Richards, R. L.; Sanders, J. R. *J. Chem. Soc., Dalton Trans.* **1998**, 2191−2198.
(35) Herwig, W.; Zeiss, H. H. *J. Org. Chem* **1958**, *23*, 1404−1404.
(36) Davies, S. C.; Hughes, D. L.; Leigh, G. J.; Sanders, J. R.; deSouza, J. S. *J. Chem. Soc., Dalton Trans.* **1997**, 1981−1988.

Table 1. Crystal Data and Structure Refinement for Li[PNP], **3**, **5**, **6**, **8**, and **9**

	Li[PNP]	$[N_2P_2]TiCl_2$ (**3**)	$[N_2P_2]CrCl_2$ (**5**)	$[N_2P_2]MnCl$ (**6**)	$[N_2P_2]CoCl$ (**8**)	$[N_2P_2]NiBr$ (**9**)
empirical formula	$C_{16}H_{36}LiNP_2$	$C_{22}H_{51}Cl_2N_2P_2SiTi$	$C_{22}H_{51}Cl_2CrN_2P_2Si$	$C_{22}H_{51}ClMnN_2P_2Si$	$C_{22}H_{51}ClCoN_2P_2Si$	$C_{22}H_{51}BrN_2NiP_2Si$
fw	311.34	552.48	556.58	524.07	528.06	572.30
T (K)	141(2)	127(2)	163(2)	130(2)	142(2)	156(2)
space group	$P2_1/c$	$P2_1/c$	$P\bar{1}$	$Pca2_1$	$P2_1/c$	$P2_1/c$
a (Å)	13.935(3)	15.900(4)	8.323(5)	23.337(3)	17.052(3)	16.555(3)
b (Å)	9.6238(19)	8.003(2)	11.887(7)	16.667(2)	11.340(2)	11.593(2)
c (Å)	30.537(6)	24.274(6)	16.425(1)	14.9432(19)	14.777(3)	14.908(3)
α (deg)	90	90	100.665(10)	90	90	90
β (deg)	99.947(3)	96.056(4)	103.110(10)	90	92.967(3)	92.564(3)
γ (deg)	90	90	108.597(10)	90	90	90
V (Å^3)	4033.8(4)	3071.5(13)	1440.4(15)	5812.2(13)	2853.5(9)	2858.4(8)
Z	8	4	2	8	4	4
λ (Å)	0.71073	0.71073	0.71073	0.71073	0.71073	0.71073
μ (cm^{-1})	0.208	0.608	0.748	0.709	0.861	2.24
$R(F_o)$ (%)	5.00	7.27	5.14	4.55	5.59	4.67
$R_w(F_o)$ (%)	10.14	19.05	11.17	9.67	14.08	10.01

was stirred for 12 h over which time the solution became forest green. The solvent was removed in vacuo, and the product was extracted with toluene. The resulting solution was concentrated and cooled to −40 °C, resulting in the formation of blue needles (0.15 g, 42% yield). IR (cm^{-1}): 1340 (m); 1301 (w); 1244 (m); 1202 (m); 1055 (m); 1019 (w); 971 (w); 926 (w); 886 (w); 847 (s); 796 (m); 756 (m); 737 (m); 655 (w); 595 (w); 519 (w). Anal. Calcd for $H_{51}C_{22}N_2P_2SiCoCl$: C, 50.03; H, 9.75; N, 5.31. Found: C, 50.00; H, 9.83; N, 5.18. Mp = 182−183 °C. μ_{eff} = 4.1 μ_B.

$[N_2P_2]$NiBr (9). To a tan suspension of $NiBr_2$ (0.15 g, 0.68 mmol) in 10 mL of DME was added a solution of **2** (0.30 g, 0.68 mmol) in 5 mL of DME dropwise at room temperature. The solution was stirred for 12 h over which time the solution turned red-brown. Following the removal of solvent under vacuum, the product was extracted with toluene, and the resulting solution was concentrated until crystalline material began precipitating. The solution was cooled to −40 °C, resulting in the formation of golden-brown crystals (0.23 g, 59% yield). IR (cm^{-1}): 1347 (m); 1242 (m); 1205 (m); 1095 (m); 1021 (m); 971 (w); 929 (w); 915 (w); 887 (w); 847 (s); 793 (m); 760 (m); 734 (s); 686 (w); 657 (w); 605 (w). Anal. Calcd for $H_{51}C_{22}N_2P_2SiNiBr$: C, 46.16; H, 9.00; N, 4.90. Found: C, 46.24; H, 9.36; N, 5.25. Mp = 142−143 °C. μ_{eff} = 2.9 μ_B.

Crystallographic Analysis. Single crystals of Li[PNP], **3**, **5**, **6**, **8**, and **9** were coated in Paratone-N oil, mounted on a Kaptan loop, transferred to a Siemens SMART diffractometer or a Bruker APEX CCD area detector,[37] centered in the beam, and cooled by a nitrogen-flow low-temperature apparatus that had been previously calibrated by a thermocouple placed at the same position as that of the crystal. Preliminary orientation matrices and cell constants were determined by the collection of 60 30 s frames, followed by spot integration and least-squares refinement. An arbitrary hemisphere of data was collected, and the raw data were integrated using *SAINT*.[38] Cell dimensions reported were calculated from all reflections with $I > 10\sigma$. The data were corrected for Lorentz and polarization effects, but no correction for crystal decay was applied. Data were analyzed for agreement and possible absorption using *XPREP*.[39] An empirical absorption correction based on comparison of redundant and equivalent reflections was applied using *SADABS*.[40] The structures were solved using *SHELXS*[41] and refined on all data by full-matrix least squares with *SHELXL-97*.[42] Thermal parameters for all non-hydrogen atoms were refined anisotropically. ORTEP diagrams were created using ORTEP-3. A summary of the X-ray diffraction data is presented in Table 1.

Results and Discussion

Ligand Synthesis and Characterization. The synthesis and characterization of Li[PNP] (the immediate precursor to our $[N_2P_2]$ ligand) was reported by Edwards and coworkers in 1989.[22] Our curiosity regarding the solid-state structure of this starting material in relation to our subsequent $[N_2P_2]$ chemistry led us to carry out an X-ray diffraction study, the results of which can be seen in Figure 3, with selected bond lengths and angles provided in Table 2. Similar to its coordination chemistry with electropositive transition metals,[18−21] the lithium salt adopts a dimeric structure with each lithium atom lying in a distorted tetrahedral environment bound by two phosphines (one from each of the two PNP moieties) as well as by both anionic nitrogen. Though we considered this a potential drawback when designing the $[N_2P_2]$ ligand, we believed the incorporation of a fourth donor would discourage such aggregation.

The anionic component of the $[N_2P_2]$ ligand was introduced by the metathesis reaction of Li[PNP] and $ClSiMe_2NH^tBu$ in pentane (Scheme 1). Following filtration and removal of volatiles under vacuum, $H[N_2P_2]$ (**1**) was isolated as a spectroscopically pure, colorless oil in 91% yield. Further reaction of **1** with 2.9 M BuLi in pentane resulted in the generation of $Li[N_2P_2]$ (**2**), which was obtained in 83% yield following crystallization as a colorless solid. Compound **2** is highly soluble in hydrocarbon and ethereal solvents and can be stored indefinitely under air-free conditions.

Synthesis and Characterization of Metal−Halide Complexes. Two similar metathesis routes were utilized in the

(37) *SMART Area-Detector Software Package*; Bruker Analytical X-ray Systems, Inc.: Madison, WI, 2001−2003.
(38) *SAINT SAX Area-Detector Integration Program*, version 6.40; Bruker Analytical X-ray Systems, Inc.: Madison, WI, 2003.
(39) *XPREP*, version 6.12, part of the *SHELXTL Crystal Structure Determination Package*; Bruker Analytical X-ray Systems, Inc.: Madison, WI, 2001.
(40) *SADABS Bruker-Nonius Area Detector Scaling and Absorption*, version 2.05; Bruker Analytical X-ray Systems, Inc.: Madison, WI, 2003.
(41) *XS Program for the Refinement of X-ray Crystal Structures*, part of the *SHELXTL Crystal Structure Determination Package*; Bruker Analytical X-ray Systems Inc.: Madison, WI, 1995−99.
(42) *XL Program for the Refinement of X-ray Crystal Structures*, part of the *SHELXT Crystal Structure Determination Package*; Bruker Analytical Systems, Inc.: Madison, WI, 1995−99.

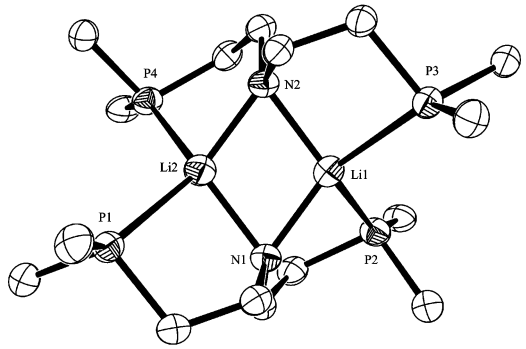

Figure 3. Thermal ellipsoid (50%) plot of Li[PNP]. Hydrogen atoms and isopropyl groups have been omitted for clarity.

Table 2. Selected Bond Lengths (Å) and Angles (deg) for Li[PNP]

Li(1)−N(1)	1.988(5)	Li(1)−N(2)	2.033(5)
Li(1)−Li(2)	2.397(6)	Li(1)−P(2)	2.550(5)
Li(1)−P(3)	2.613(5)	Li(2)−N(2)	1.990(5)
Li(2)−N(1)	2.035(5)	Li(2)−P(4)	2.555(5)
Li(2)−P(1)	2.594(5)		
N(1)−Li(1)−N(2)	106.7(2)	N(1)−Li(1)−Li(2)	54.33(17)
N(2)−Li(1)−Li(2)	52.61(17)	N(1)−Li(1)−P(2)	82.21(18)
N(2)−Li(1)−P(2)	134.2(2)	Li(2)−Li(1)−P(2)	114.8(2)
N(1)−Li(1)−P(3)	137.8(2)	N(2)−Li(1)−P(3)	87.00(18)
Li(2)−Li(1)−P(3)	128.3(2)	P(2)−Li(1)−P(3)	116.75(17)
N(2)−Li(2)−N(1)	106.5(2)	N(2)−Li(2)−Li(1)	54.24(17)
N(1)−Li(2)−Li(1)	52.53(16)	N(2)−Li(2)−P(4)	83.78(17)
N(1)−Li(2)−P(4)	132.7(2)	Li(1)−Li(2)−P(4)	115.0(2)
N(2)−Li(2)−P(1)	135.7(2)	N(1)−Li(2)−P(1)	87.36(18)
N(1)−Li(2)−P(1)	127.3(2)	P(4)−Li(2)−P(1)	117.52(17)

Scheme 1

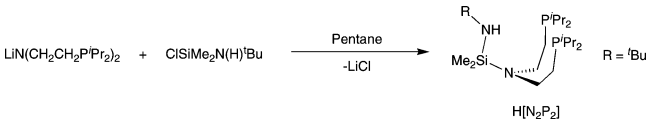

Scheme 2

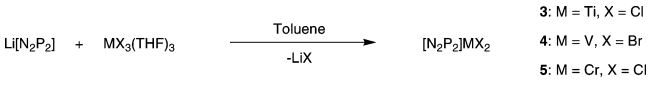

Scheme 3

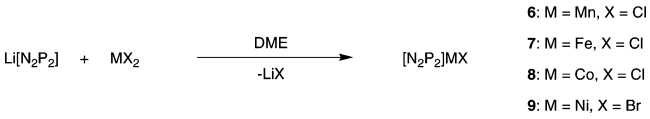

synthesis of seven new first-row transition-metal complexes supported by the [N_2P_2] ligand. While initial reactions were performed in THF, we discovered that much cleaner reactions and higher yields were obtained when toluene or DME were used as solvents. For titanium, vanadium, and chromium, the trivalent THF adduct starting materials $MX_3(THF)_3$ were combined in toluene with **2** at room temperature, and following workup, crystalline material of each was isolated (Scheme 2). With manganese, iron, cobalt, and nickel, the reaction of MX_2 and **2** in DME at room temperature was found to be a sufficient method of synthesis (Scheme 3).

For [N_2P_2]$TiCl_2$ (**3**), turquoise crystals were grown from a toluene solution at −40 °C, and the product was isolated in 56% yield. Recrystallization of **3** from diethyl ether gave crystals suitable for an X-ray diffraction study, and the results are shown in Figure 4, with selected bond lengths and angles

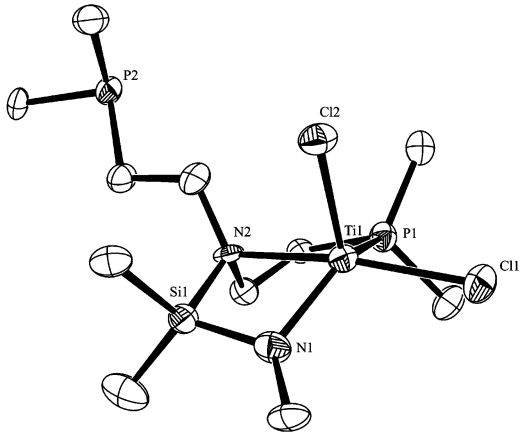

Figure 4. Thermal ellipsoid (50%) plot of **3**. Hydrogen atoms and isopropyl methyl and *tert*-butyl methyl groups have been omitted for clarity.

Table 3. Selected Bond Lengths (Å) and Angles (deg) for **3**

Ti(1)−Cl(1)	2.332(2)	Ti(1)−Cl(2)	2.314(2)
Ti(1)−N(1)	1.972(4)	Ti(1)−N(2)	2.356(6)
Ti(1)−P(1)	2.594(2)		
Cl(1)−Ti(1)−Cl(2)	102.40(7)	Cl(1)−Ti(1)−N(1)	112.4(2)
Cl(1)−Ti(1)−N(2)	158.6(1)	Cl(1)−Ti(1)−P(1)	86.69(6)
Cl(2)−Ti(1)−N(1)	110.7(2)	Cl(2)−Ti(1)−N(2)	95.4(1)
Cl(2)−Ti(1)−P(1)	114.88(6)	N(1)−Ti(1)−N(2)	71.2(2)
N(1)−Ti(1)−P(1)	124.8(1)	N(2)−Ti(1)−P(1)	75.0(1)
N(1)−Si(1)−N(2)	93.5(2)		

provided in Table 3. The titanium atom lies in a distorted square-based pyramid geometry with two terminal chlorides and the [N_2P_2] ligand bound κ^3-N_2P. One phosphine donor remains uncoordinated in the solid state even though an open coordination site appears to exist on the titanium atom at the base of the pyramid, as evidenced by the crystal structure. The preference for five-coordinate over a six-coordinate geometry appears to be strong in this particular case. The Ti−Cl bond lengths of 2.332(2) and 2.314(2) Å are similar to those found in six-coordinate [$O(CH_2CH_2OMe)_2$]$TiCl_3$ (2.343(6), 2.326(7), and 2.323(6) Å),[43] and the neutral Ti−N bond length of 2.356(5) Å is similar to the values observed in $TiCl_3$(TMEDA)(THF) (2.281(5) and 2.343(4) Å).[44] The anionic Ti−N bond distance (1.972(4) Å) is slightly longer than the length found in the related compound [P_2N_2]$TiCl_2$,[45] where [P_2N_2] = $PhP(CH_2SiMe_2NSiMe_2CH_2)_2PPh$, which has bond distances of 1.914(3) and 1.936(4) Å, as expected given the higher oxidation state of the latter. The neutral Ti−P bond distance of 2.594(2) Å is also comparable to those of other Ti(III) phosphine complexes such as [Ti(μ-Cl)$_2$$Cl_2$-(depe)] (2.604(1) and 2.610(1) Å).[46] Another interesting feature of the solid-state structure of **3** is the distorted N(1)−Si(1)−N(2) bond angle of 93.5(2)°. Though this angle is greatly distorted from the ideal tetrahedral angle of 109.5° and a four-membered ring is formed upon complexation of the ligand, this small angle does not appear to indicate the

(43) Drew, M. G. B.; Hutton, J. A. *J. Chem. Soc., Dalton Trans.* **1978**, 1176−1179.
(44) Oshiki, T.; Kiriyama, T.; Tsuchida, K.; Takai, K. *Chem. Lett.* **2000**, 334−335.
(45) Morello, L.; Yu, P. H.; Carmichael, C. D.; Patrick, B. O.; Fryzuk, M. D. *J. Am. Chem. Soc.* **2005**, *127*, 12796−12797.
(46) Cotton, F. A.; Murillo, C. A.; Petrukhina, M. A. *J. Organomet. Chem.* **1999**, *573*, 78−86.

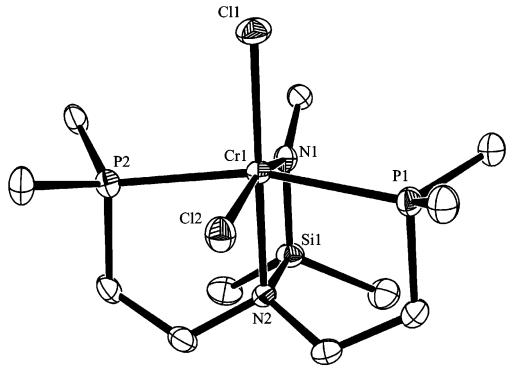

Figure 5. Thermal ellipsoid (50%) plot of **5**. Hydrogen atoms and isopropyl methyl and *tert*-butyl methyl groups have been omitted for clarity.

Table 4. Selected Bond Lengths (Å) and Angles (deg) for **5**

Cr(1)−Cl(1)	2.303(2)	Cr(1)−Cl(2)	2.389(1)
Cr(1)−N(1)	2.048(3)	Cr(1)−N(2)	2.134(3)
Cr(1)−P(1)	2.458(1)	Cr(1)−P(2)	2.484(1)
Cl(1)−Cr(1)−Cl(2)	92.76(4)	Cl(1)−Cr(1)−N(1)	103.56(9)
Cl(1)−Cr(1)−N(2)	179.3(1)	Cl(1)−Cr(1)−P(1)	95.73(4)
Cl(1)−Cr(1)−P(2)	95.71(4)	Cl(2)−Cr(1)−N(1)	163.64(9)
Cl(2)−Cr(1)−N(2)	87.87(10)	Cl(2)−Cr(1)−P(1)	84.26(4)
Cl(2)−Cr(1)−P(2)	82.90(4)	N(1)−Cr(1)−N(2)	75.8(1)
N(1)−Cr(1)−P(1)	92.93(10)	N(1)−Cr(1)−P(2)	96.32(10)
N(2)−Cr(1)−P(1)	84.65(9)	N(2)−Cr(1)−P(2)	84.04(9)
P(1)−Cr(1)−P(2)	163.17(4)	N(1)−Si(1)−N(2)	93.6(1)

inability of both phosphine donors to bind to the metal center (see below) and further suggests the ligand only binds κ^3-N_2P to fulfill the electron needs of the metal center. The observed magnetic moment ($\mu_{eff} = 1.3\ \mu_B$) falls below the expected spin-only value of 1.7 μ_B for a d^1 compound. This measurement was reproducible in solution using the Evans method[47] as well as in the solid-state using a Johnson Matthey magnetic susceptibility balance.

The compound $[N_2P_2]VBr_2$ (**4**) was isolated in 54% yield as blue-green crystals following crystallization from a solution of THF at −40 °C. Though numerous attempts were made, X-ray quality crystals could not be isolated, and the coordination mode of the ligand could not be determined. The elemental analysis was consistent with the proposed formulation of **4**, and the solid-state magnetic moment was found to be 2.7 μ_B, consistent with a d^2 high-spin complex.

Purple crystals of $[N_2P_2]CrCl_2$ (**5**) were grown from a diethyl ether solution at −40 °C and isolated in 48% yield. The solid-state structure of **5** is shown in Figure 5, with selected bond lengths and angles provided in Table 4. In contrast to the case in **3**, the chromium atom in **5** is octahedral with the $[N_2P_2]$ ligand bound κ^4-N_2P_2 to the metal center. The Cr−Cl bond distances of 2.303(2) and 2.389(1) Å differ likely due to π donation from the lone pair of electrons on the anionic nitrogen donor leading to a longer trans bond length; however, they are comparable to those in the related compounds $[CrCl\{N(CH_2CH_2PMe_2)_2\}]$[20] (2.401(1) Å) and H[PNP]$CrCl_3$[25] (2.2898(10), 2.3090(11), and 2.3616(11) Å). The Cr−P bond distances (2.458(1) and 2.484(1) Å) also correlate well with the lengths observed in the aforementioned systems. The Cr−N bond distances in **5** (2.048(3) and 2.134(3) Å) also agree well with those found in the literature.[20] Again, as in **3**, the N(1)−Si(1)−N(2) angle of 93.6(1)° is greatly distorted from tetrahedral; however, the observation that $[N_2P_2]$ can bind κ^4-N_2P_2 to chromium and still have a greatly distorted angle about the silicon atom further suggests the binding of the second neutral phosphine may be related more to the electronic requirements of the metal center than to some restriction found in the design of the ligand. The solid-state magnetic moment of **5** was found to be 3.9 μ_B and is in the expected range for a d^3 high-spin complex.

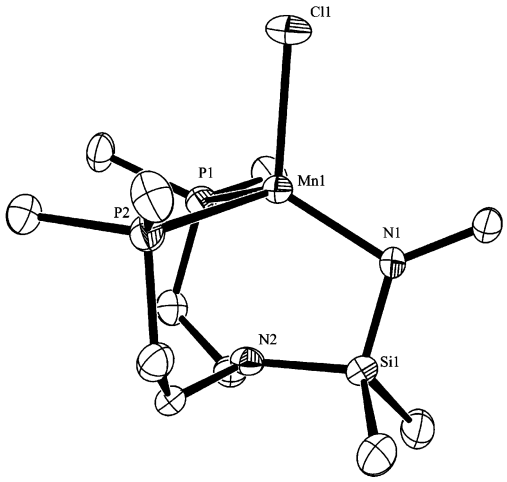

Figure 6. Thermal ellipsoid (50%) plot of **6**. Hydrogen atoms and isopropyl methyl and *tert*-butyl methyl groups have been omitted for clarity.

Table 5. Selected Bond Lengths (Å) and Angles (deg) for **6**

Mn(1)−Cl(1)	2.385(1)	Mn(1)−N(1)	2.029(4)
Mn(1)−P(1)	2.601(1)	Mn(1)−P(2)	2.582(1)
Cl(1)−Mn(1)−N(1)	118.3(1)	Cl(1)−Mn(1)−P(1)	100.24(5)
Cl(1)−Mn(1)−P(2)	103.00(5)	N(1)−Mn(1)−P(1)	117.3(1)
N(1)−Mn(1)−P(2)	111.6(1)	P(1)−Mn(1)−P(2)	104.44(5)
N(1)−Si(1)−N(2)	102.3(2)		

Colorless crystals of $[N_2P_2]MnCl$ (**6**) were isolated in 56% yield following crystallization from a toluene solution at −40 °C. Needles of **6** suitable for an X-ray diffraction study were grown from a DME solution at −40 °C, and an ORTEP representation is shown in Figure 6, with selected bond lengths and angles provided in Table 5. Unlike the coordination modes observed in the cases of **3** and **5**, in **6** the $[N_2P_2]$ ligand is coordinated κ^3-NP_2 to manganese by the two neutral phosphines and the anionic nitrogen donor. The resulting geometry about the manganese atom falls between tetrahedral and trigonal bipyramidal with Cl(1)−Mn(1)−P(1), Cl(1)−Mn(1)−P(2), and Cl(1)−Mn(1)−N(1) angles of 100.24(5)°, 103.00(5)°, and 118.3(1)°, respectively. Though the basal nitrogen is uncoordinated in the solid-state, there may be some interaction with the manganese atom in solution. In contrast to that of the related compound $[PhBP^{iPr}_3]MnCl$ ($[PhBP^{iPr}_3] = PhB(CH_2P^iPr_2)_3$) where the metal lies in a distorted tetrahedral environment with Cl−Mn−P angles of 125.38(2)°, 120.22(2)°, and 126.14(2)°,[48] the geometry of **6** is more compressed than elongated from tetrahedral. This

(47) Piguet, C. *J. Chem. Educ.* **1997**, *74*, 815−816.

(48) Lu, C. C.; Peters, J. C. *Inorg. Chem.* **2006**, *45*, 8597−8607.

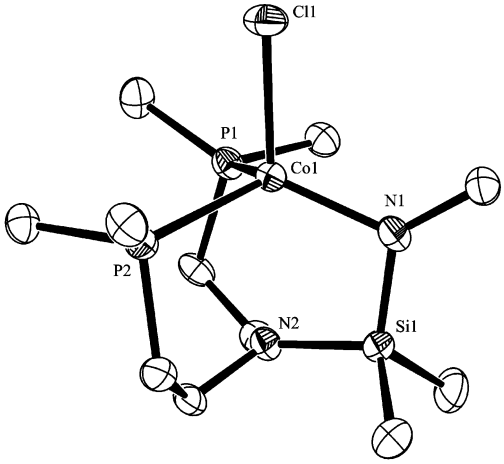

Figure 7. Thermal ellipsoid (50%) plot of **8**. Hydrogen atoms and isopropyl methyl and *tert*-butyl methyl groups have been omitted for clarity.

Table 6. Selected Bond Lengths (Å) and Angles (deg) for **8**

Co(1)−Cl(1)	2.319(2)	Co(1)−N(1)	1.965(5)
Co(1)−P(1)	2.397(2)	Co(1)−P(2)	2.393(2)
Cl(1)−Co(1)−N(1)	113.1(1)	Cl(1)−Co(1)−P(1)	102.76(6)
Cl(1)−Co(1)−P(2)	99.67(6)	N(1)−Co(1)−P(1)	112.7(1)
N(1)−Co(1)−P(2)	117.3(1)	P(1)−Co(1)−P(2)	109.64(5)
N(1)−Si(1)−N(2)	101.4(2)		

move toward a trigonal bipyramidal geometry may have some meaningful consequences. Interaction with the basal nitrogen may account for the substantial elongation of the Mn−Cl bond (2.385(1) Å) in **6** compared with that observed in [$PhBP^{iPr}_3$]MnCl (2.2687(7) Å). The Mn−P distances of 2.601(1) and 2.582(1) Å are also longer than those found in the former compound (2.5300(6), 2.5298(6), and 2.5289(6) Å). The solid-state magnetic moment was found to be 5.8 μ_B, indicating a high-spin d^5 configuration.

Yellow needles of [N_2P_2]FeCl (**7**) and blue-green crystals of [N_2P_2]CoCl (**8**) were both grown from toluene solutions at −40 °C and were isolated in 61 and 42% yields, respectively. Single-crystal X-ray diffraction studies revealed that the solid-state structures of **7** and **8** are isomorphic; however, crystals of **7** were twinned and only the connectivity could be determined. Therefore, while only the structure of **8** will be considered here, general geometric and structural features appear to be similar in both compounds. Crystals of **8** suitable for an X-ray diffraction study were grown from a toluene solution at −15 °C, and a thermal ellipsoid plot of **8** is shown in Figure 7, with selected bond lengths and angles provided in Table 6. Analogous to **6**, the [N_2P_2] ligand is bound κ^3-NP_2, and the geometry of the complex is distorted tetrahedral with Cl(1)−Co(1)−P(1), Cl(1)−Co(1)−P(2), and Cl(1)−Co(1)−N(1) angles of 102.76(6)°, 99.67(6)°, and 113.1(1)°, respectively. The Co−Cl bond distance of 2.319(2) Å is longer than the lengths observed in the related Co(II) tetrahedral complexes [$Co(np_3)Cl]PF_6$[49] (2.225(4) Å), $CoCl_2\{H_3CN(CH_2CH_2PPh_2)_2\}$[50] (2.2483(16) and 2.2817(16) Å), and [$PhBP^{iPr}_3$]CoCl[51] (2.196(3) Å). As suggested in the case of **6**, elongation of the M−Cl bond may result from interaction of the basal nitrogen with the metal center. The

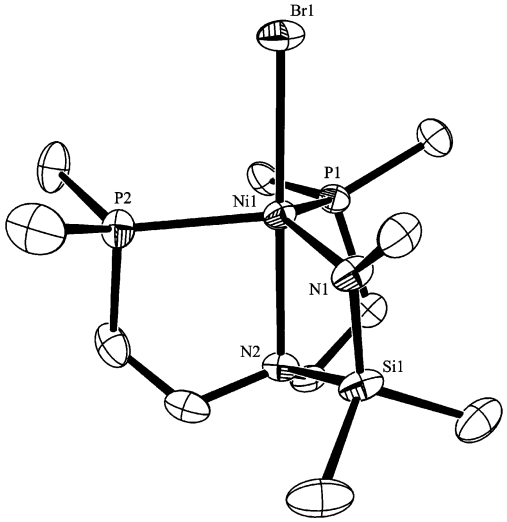

Figure 8. Thermal ellipsoid (50%) plot of **9**. Hydrogen atoms and isopropyl methyl and *tert*-butyl methyl groups have been omitted for clarity.

Table 7. Selected Bond Lengths (Å) and Angles (deg) for **9**

Ni(1)−Br(1)	2.5627(7)	Ni(1)−N(1)	1.934(3)
Ni(1)−N(2)	2.280(3)	Ni(1)−P(1)	2.361(1)
Ni(1)−P(2)	2.346(1)		
Br(1)−Ni(1)−N(1)	105.11(10)	Br(1)−Ni(1)−N(2)	177.53(9)
Br(1)−Ni(1)−P(1)	94.07(3)	Br(1)−Ni(1)−P(2)	96.14(4)
N(1)−Ni(1)−N(2)	76.4(1)	N(1)−Ni(1)−P(1)	124.2(1)
N(1)−Ni(1)−P(2)	122.5(1)	N(2)−Ni(1)−P(1)	83.46(9)
N(2)−Ni(1)−P(2)	84.51(9)	P(1)−Ni(1)−P(2)	106.28
N(1)−Si(1)−N(2)	97.9(2)		

Co−P bond distances (2.397(2) and 2.393(2) Å) are equivalent within error and are similar to those found in the literature. The observed magnetic moments of **7** and **8** indicated both are high-spin species and were found to be 4.9 and 4.1 μ_B, respectively.

Golden-brown crystals of [N_2P_2]NiBr (**9**) were isolated in 59% yield following crystallization from a toluene solution at −40 °C. Recrystallization from a DME solution at −40 °C resulted in the formation of needle-like crystals suitable for an X-ray diffraction study, and an ORTEP diagram of **9** is shown in Figure 8, with selected bond lengths and angles provided in Table 7. In contrast to **6** and **8**, the geometry of the nickel atom in **9** is trigonal bipyramidal, with the [N_2P_2] ligand bound κ^4-N_2P_2 as was observed in **5**. The Ni−Br bond distance of 2.5627(7) Å is significantly longer than those observed in [NiL^2Br_2],[52] where L^2 = 2,6-bis(methylthiomethyl)pyridine, with bond lengths of 2.434(1) and 2.417(1) Å. The neutral (2.280(3) Å) and anionic (1.934(3) Å) Ni−N bond distances differ significantly in **9**; however, both agree well with literature values.[53,54] The Ni−P bond distances of 2.361(1) and 2.346(1) Å are longer than those observed in the related compound (^{R}PNP)NiCl[53] (2.2086(6) and 2.1975-

(49) Di Vaira, M.; Orlandini, A. B. *Inorg. Chem.* **1973**, *12*, 1292−1297.
(50) Wang, M.; Yu, X. M.; Shi, Z.; Qian, M. X.; Jin, K.; Chen, J. H.; He, R. *J. Organomet. Chem.* **2002**, *645*, 127−133.
(51) Betley, T. A.; Peters, J. C. *Inorg. Chem.* **2003**, *42*, 5074−5084.
(52) Ball, R. J.; Genge, A. R. J.; Radford, A. L.; Skelton, B. W.; Tolhurst, V. A.; White, A. H. *Dalton Trans.* **2001**, 2807−2812.
(53) Fryzuk, M. D.; Macneil, P. A.; Rettig, S. J.; Secco, A. S.; Trotter, J. *Organometallics* **1982**, *1*, 918−930.
(54) Hou, J. X.; Sun, W. H.; Zhang, S.; Ma, H. W.; Deng, Y.; Lu, X. M. *Organometallics* **2006**, *25*, 236−244.

(5) Å) possibly due to the substitution of electron-withdrawing phenyl groups for more electron-releasing isopropyl groups in addition to a fourth donor arm. Also of note is the N(1)−Si(1)−N(2) angle of 97.9(2)°, which is less distorted from tetrahedral than the values observed in **3** and **5** but again appears to have little bearing on the coordination mode of the ligand. The magnetic moment was found to be 2.9 μ_B, well in the expected range for a high-spin Ni(II) compound.

Electrochemistry. Cyclic voltammetry (CV) studies of compounds **3**−**9** were carried out in dichloromethane with [*n*Bu_4N][PF_6] (0.3 M) as the supporting electrolyte. The CV of **3** displays a reversible one-electron oxidation to Ti(IV) at −0.350 V and an irreversible reduction at −2.28 V. Similarly, the CV of **4** reveals two electrochemical processes, one being an irreversible oxidation at +0.190 V and the other an irreversible reduction at −1.27 V. When we compare the electrochemical data from our previous work with the TDMA ligand BPPA to those obtained from the current system supported by [N_2P_2], we see that the [N_2P_2] ligand is less electron releasing than BPPA in the case of Ti(III) and V(III).[30] A number of factors likely contribute to this observation such as the substitution of hard pyridyl donors for softer phosphines and the possible lower coordination number in solution for [N_2P_2] compared with BPPA.

The CV of **5** shows two electrochemical processes. The first is a reversible one-electron reduction for the Cr(II)/Cr(III) couple at −1.42 V, and the second is an asymmetric oxidation couple at −0.232 V. Both couples are followed by further electrochemical processes. No active reductive process in the solvent window examined (dichloromethane) was observed in the CV of **6**; however, the CV does reveal a reversible oxidation for the Mn(II)/Mn(III) couple at −0.194 V.

Two irreversible reactions are revealed in the CV of **7** with a reduction of Fe(II) at −1.68 V as well as an oxidation at −0.156 V followed by further electrochemical oxidations. Similar results were observed with the related compound [$^{Si}NP_2$]FeCl[28] with an irreversible reduction at −2.1 V and an irreversible oxidation at +0.24 V. In contrast, the CV of **8** shows a reversible reduction at −1.4 V and an irreversible oxidation at −0.17 V. The more electron-releasing nature of [N_2P_2] with cobalt compared with that of [$^{Si}NP_2$][28] may possibly be due to the interaction of the free lone pair of electrons on the basal nitrogen with the metal center.

Electrochemical studies of **9** show two irreversible electrochemical reactions: a reduction at −1.02 V and an oxidation at +0.411 V. Both processes are followed by additional electrochemical reactions. The CV of the related compound [PhB^{iPr}_3]NiCl displays a reversible reduction for the Ni(I)/Ni(II) couple at −1.4 V, suggesting that [PhB^{iPr}_3] is more electron releasing, which can be attributed to its zwitterionic nature.

Conclusions

The incorporation of neutral phosphines into the previous TDMA ligand design allowed for the synthesis of the new multidentate ligand [N_2P_2]. The [N_2P_2] ligand demonstrates the flexibility to adapt to the electronic needs of the metal center it supports by coordinating in one of three distinct modes, as either a tridentate (κ^3-N_2P, κ^3-NP_2) or a tetradentate (κ^4-N_2P_2) ligand. We believe this characteristic, along with the good yields, stability, and good solubility of this class of complexes will allow for the study of new and interesting reduced metal complexes as well as reactive organometallic species. Work in progress along these lines will be the subject of subsequent papers.[55]

Acknowledgment. We are grateful to the National Science Foundation for financial support for this work and Dr. Fred Hollander for crystallographic assistance.

Note Added after ASAP Publication. This article was released ASAP on December 1, 2007, with incorrect references to Figures 9 and 10 in the text. The correct version was posted on December 4, 2007.

Supporting Information Available: Crystallographic information files (CIF). This material is available free of charge via the Internet at http://pubs.acs.org.

IC701670U

(55) Chomitz, W. A.; Arnold, J. *Chem. Commun.* **2007**, 4797−4799.